Sea salt emission, transportation and influence on nitrate simulation: a case study in Europe

Ying Chen[1,2], Yafang Cheng[2], Nan Ma[1,2], Ralf Wolke[1], Stephan Nordmann[3], Stephanie Schüttauf[1], Liang Ran[4], Birgit Wehner[1], Wolfram Birmili[3], Hugo A. C. Denier van der Gon[5], Qing Mu[2], Stefan Barthel[1], Gerald Spindler[1], Bastian Stieger[1], Konrad Müller[1], Guang-Jie Zheng[6], Ulrich Pöschl[2], Hang Su[2] and Alfred Wiedensohler[1]

[1]Leibniz-Institute for Tropospheric Research, Leipzig, 04318, Germany
[2]Multiphase Chemistry Department, Max Planck Institute for Chemistry, Mainz, 55128, Germany
[3]German Environment Agency, Dessau-Roßlau, 06844, Germany
[4]Key Laboratory of Middle Atmosphere and Global Environment Observation, Institute of Atmospheric Physics, Chinese Academy of Sciences, Beijing, 100029, China
[5]TNO, Dept. of Climate, Air and Sustainability, Princetonlaan 6, 3584 CB Utrecht, the Netherlands
[6]State Key Joint Laboratory of Environment Simulation and Pollution Control, School of Environment, Tsinghua University, Beijing 100084, China

Correspondence to: Y. Cheng (yafang.cheng@mpic.de) and Y. Chen (chen@tropos.de)

Abstract. Sea salt aerosol (SSA) is one of the major components of primary aerosols and has significant impact on the formation of secondary inorganic aerosol particles on a global scale. In this study, the fully online coupled WRF-Chem model was utilized to evaluate the SSA emission scheme and its influence on the nitrate simulation in a case study in Europe during September 10-20, 2013. Meteorological conditions near the surface, wind pattern, and thermal stratification structure were well reproduced by the model. Nonetheless, coarse mode (PM_{1-10}) particle mass concentration was substantially overestimated due to the overestimation of SSA and nitrate. Compared to filter measurements at 4 EMEP stations (coastal stations: Bilthoven, Kollumerwaard and Vredepeel; inland station: Melpitz), the modeled SSA concentrations were overestimated by a factor of 8-20. We found that the overestimation was mainly caused by the overestimated SSA emission over North Sea during September 16-20. Over the coastal regions, the SSA was injected into the continental free troposphere through an "aloft bridge" (about 500 to 1000 meter above the ground), a result of the different thermodynamic properties and planetary boundary layer (PBL) structure between continental and marine regions. The injected SSA was further transported inland and mixed downward to the surface through downdraft and PBL turbulence. This process broadened the influence of SSA to a larger downwind region, for example, leading to an overestimation of SSA at Melpitz, Germany by a factor of ~20. As a result, nitrate partitioning fraction (ratio between particulate nitrate and the summation of particulate nitrate and gas-phase nitric acid) increased by about 0.2 for the coarse mode nitrate due to the overestimation of SSA at Melpitz, but no significant difference in the partitioning fraction for the fine mode nitrate. About 140% overestimation of the coarse mode nitrate was resulted from the influence of SSA at Melpitz. On the other hand, the overestimation of SSA inhibited the nitrate formation in the fine mode by about 20%, because of the increased consumption of precursors by coarse mode nitrate formation.

1 Introduction

Atmospheric aerosol plays an important role in climate change (IPCC, 2013). Further they have an adverse effect on human health (Pope et al., 2009). Aerosol particles could either be primarily emitted or secondarily produced. Sea-salt aerosol (SSA) is one major constitute of primary natural aerosol particles on the global scale

(Lewis, 2004), possibly comparable with mineral dust particles in the Northern Hemisphere (IPCC, 2013; Mårtensson et al., 2010). SSA is mainly produced by bursting bubbles during whitecap formation in the open ocean (Monahan et al., 1986). Waves breaking in the surf zone, where has more whitecaps and stronger emission due to increasing ocean bottom and higher intensity of wave breaking, may affect areas at a distance

5   of 25 km from the coastline and can dominate the coastal region (de Leeuw et al., 2000; Monahan, 1995; Woodcock et al., 1963).

SSA could participate in heterogeneous reactions by interacting with trace gases, leading to the formation of secondary aerosols (Seinfeld, 2006), such as nitrate, which is one of the most important secondary inorganic aerosol and is the dominant aerosol component in western and central Europe (Schaap et al., 2011). SSA has a

10   significant influence on nitrate formation as shown in previous studies (Neumann et al., 2016; Liu et al., 2015; Im, 2013; Athanasopoulou et al., 2008). Sodium nitrate is produced with a chloride deficit in the SSA (Schaap et al., 2011; Seinfeld, 2006), and the timescale of the corresponding reaction is about several hours (Meng and Seinfeld, 1996). As reported in previous studies, sodium nitrate is largely contributed to nitrates in northern and southern Europe (Pakkanen et al., 1999), whereas in western and central Europe ammonium nitrate dominates

15   (Schaap et al., 2002; ten Brink et al., 1997).

Usually, SSA has a short life-time due to its quick deposition within the coastal region (Grythe et al., 2014), thus its influence on nitrate formation cannot reach the distant inland area. However, local circulations can change the vertical distributions of aerosol particles and make the long-range transport of SSA possible by lifting up aerosol from the planetary boundary layer (PBL) into the free troposphere (Chen et al., 2009; Dacre et al., 2007;

20   Lu and Turco, 1995, 1994). The development of PBL or downdraft over the continent could later on drag the lifted particles downward back to the surface (Chen et al., 2009). These mechanisms provide an opportunity for SSA to be transported inland, and thereby make their influence more extensive, from coastal to regional or even global.

SSA contributes much more to the global aerosol burden than anthropogenic aerosol does. However in terms of

25   global mass, SSA has the largest uncertainty among all aerosols (Grythe et al., 2014). The parameterization scheme (Gong, 2003; Monahan et al., 1986) of SSA emissions in WRF-Chem is still highly uncertain (Grythe et al., 2014; Neumann et al., 2016). Previous studies (Neumann et al., 2016; Nordmann et al., 2014; Archer-Nicholls et al., 2014; Zhang et al., 2013; Saide et al., 2012; Saide et al., 2013; de Leeuw et al., 2011) showed that parameterization of Gong (2003) may overestimate the emission of SSA. Saide et al. (2012) demonstrated that

30   the SSA emissions scheme (Gong, 2003) overestimated SSA by a factor of 10 for sub-micron particles and a factor of 2 for super-microns in the southeast Pacific Ocean. Jaeglé et al. (2011) found that this SSA emission scheme overestimated coarse mode SSA mass concentrations by factors of 2–3 at high wind speeds over the cold waters of the Southern, North Pacific and North Atlantic Oceans. Other studies also indicated an overestimation of SSA emissions in varying degrees (Zhang et al., 2013; de Leeuw et al., 2011; Yang et al., 2011).

35   The accuracy of the SSA emission scheme is critical for the evaluation of the climate effect (Soares et al., 2016) and its influence on nitrate formation. The uncertainty of the SSA emission scheme directly determines the uncertainty of the evaluation of SSA radiative forcing. Additionally SSA has an indirect effect on the total aerosol burden; the heterogeneous reaction could amplify the uncertainty of total aerosol burden due to the influence of SSA on secondary aerosol formation (e.g., nitrate, Seinfeld, 2006). Such indirect effect needs the participation

40   of gaseous pollutants such as nitrogen oxides (NOx), which are not only abundant along the coast area (Fig. S1). Furthermore, the long-range transport mechanisms, as mentioned above, make the importance of SSA indirect effect on nitrate formation over a broader region.

In this study, the long-range transport mechanism and the influence of SSA over the inland region were analyzed in detail by a case study in Europe. The parameterizations of model and the observations are

45   introduced in section 2. The background meteorological conditions are described in section 3.1. Basic physical

and chemical properties obtained from model simulations were evaluated in section 3.2. The long-range transport mechanism of SSA and evaluation of SSA emission were shown in section 3.3. In section 3.4, the influence of SSA on the nitrate simulation was quantitatively analyzed.

2 Data & Methods

5   **2.1 WRF-Chem model**

The Weather Research and Forecasting/Chemistry model (WRF-Chem V3.5.1) is a fully "online" coupled regional air quality model. It is designed for a broad spectrum of atmospheric research, ranging from several hundred meters to thousands of kilometers in horizontal extent. In addition to the meteorology, aerosols, trace gases and interactive processes are simulated in the model (Grell et al., 2005).

10   In order to represent the properties of size-resolved aerosol particles, the MOdel for Simulating Aerosol Interactions and Chemistry (MOSAIC, Zaveri et al., 2008) is utilized in this study. In MOSAIC, there are eight discrete size bins (from about 39 nm to 10 μm, see Fig. S2) of dry particles. Particles are assumed to be internally-mixed in each bin (Zaveri et al., 2008). The size range of the fifth bin is from 625 nm to 1250 nm. Assuming that particle mass size distribution was constant in the fifth bin, we divided the particle mass in this

15   size bin into 60% to the fine mode (PM$_1$, diameter smaller than 1 μm) and the rest 40% to the coarse mode (PM$_{1-10}$, diameter ranging from 1 to 10 μm).

In MOSAIC, sulfate, methane sulfonate, nitrate, chloride, carbonate, ammonium, sodium, calcium, elemental carbon (EC), other inorganic material and organic carbon (OC) are all treated in each bin. Both particle mass concentrations and particle number concentrations are simulated. Since the segregation of particles in the size

20   bin is based on the dry diameter, there will be no transfer of particles between the bins due to the uptake or loss of water (Zaveri et al., 2008). However, the transfer of particles between the bins could results from the growth or shrink of particles due to chemical processes (e.g., uptake or release of trace gases, etc.) and physical processes (e.g., coagulation, etc., Chapman et al., 2009). The formation mechanism of secondary organic aerosols is not included in the chosen MOSAIC version, but the nucleation of sulfuric acid and water vapor is

25   considered (Zaveri et al., 2008; Fast et al., 2006).

Dry and wet deposition of particles is treated in the WRF-Chem model (Binkowski and Shankar, 1995). The dry deposition of particles is calculated on the basis of the sublayer resistance, aerodynamic resistance and surface resistance (Grell et al., 2005). The scavenging process of particles was calculated using look-up tables (Nordmann et al., 2014). It is worth mentioning that Saide et al. (2012) found the WRF-Chem model might

30   overestimate wet deposition of particles, in the regions where drizzles re-evaporates and release the particles back into the atmosphere.

The gas-phase atmospheric chemistry was presented by the Carbon-Bond Mechanism version Z (CBMZ), which is coupled with MOSAIC. In CBMZ, 67 prognostic species and 164 reactions are included with a lumped structure approach (Fast et al., 2006; Zaveri and Peters, 1999). Organic compounds are categorized according to their

35   internal bond types. The rates for photolytic reactions are calculated with the Fast-J scheme (Barnard et al., 2004; Wild et al., 2000).

The simulations were performed for the HOPE-Campaign (HD(CP)² Observational Prototype Experiment, https://icdc.zmaw.de/hopm.html) held at the observatory Melpitz (12.93°E, 51.53°N, 86 m a.s.l.) from September 10-20, 2013. Three nested domains with 39 vertical layers were set up for the simulated case. The

40   outer domain covers the whole Europe, part of the North Sea and the North Africa with a spatial resolution of 54 km, providing the boundary conditions for the inner domains. The innermost domain was centered at Melpitz, and had a spatial resolution of 6 km. The intermediate domain (D02, Fig. 1) was also centered at

Melpitz, and covers part of the North Sea, the central and southern Europe with a spatial resolution of 18 km. The spin-up of the model run was 2 days.

Final Analysis (FNL) Operational Global Analysis (http://rda.ucar.edu/datasets/ds083.2/) and sea surface temperature (SST) datasets (http://polar.ncep.noaa.gov/sst/oper/Welcome.html), with a spatial resolution of 1 degree and a temporal resolution of 6 hours, were utilized to drive and force the model meteorological field. The initial chemical and boundary conditions were provided by the MOZART-4 global model (http://www.acd.ucar.edu/wrf-chem/mozart.shtml) with a spatial resolution of $1.9^{o} \times 2.5^{o}$ and a temporal resolution of 6 hours. More details about setups and parameterizations of the simulation are given in Table 1.

2.2 Emissions

SSA results from dried sea spray ejected into the atmosphere from the sea surface (Lewis, 2004). Sea spray is emitted from bubble bursting or breaking waves torn by winds at wave crests. Strong winds exceeding 10 ms^{-1} are needed for the second process (Neumann et al., 2016; Monahan et al., 1986). The parameterization of SSA emission scheme coupled in WRF-Chem model follows the Gong (2003) scheme. This SSA emission scheme was developed based on the semi-empirical formulation (Monahan et al., 1986) and field measurements (O'Dowd et al., 1997), including two mechanisms of SSA production via bubbles (i.e., jet-drop and film-drop). The SSA flux between ocean and atmosphere was described as a function of 10-m wind speed and particle radius. An adjustable parameter, which controls the shape of submicron size distributions, was introduced into Gong (2003) scheme in order to improve the overestimation of submicron SSA in Monahan et al. (1986) scheme. The default value 30 was used for this adjustable parameter in WRF-Chem simulation, as recommended by Gong (2003). More detailed information about this SSA emission scheme is given by Gong (2003).

The inventory of anthropogenic emissions ($PM_{2.5}$, $PM_{2.5-10}$, CO, NOx, SO_2, NH_3 and Non-methane volatile organic compounds), as well as temporal resolved emission factors were provided by TNO for the AQMEII project (Pouliot et al., 2012). The dataset consists of European anthropogenic emissions on $1/8^{o} \times 1/16^{o}$ lon-lat grid for the whole year 2006. The Selected Nomenclature of Air Pollution (SNAP-code) was used to categorize different source types (e.g., energy transformation, industrial combustion, road transport, agriculture), with area and point emissions distinguished. More details about anthropogenic emission inventory are given in related literatures (Pouliot et al., 2012; Wolke et al., 2012).

The anthropogenic emission of EC and OC were taken from the Pan-European Carbonaceous aerosol inventory (Visschedijk and Denier van der Gon, 2008), which was developed in the framework of the European Integrated project on Aerosol Cloud Climate and Air Quality interactions (EUCAARI, Kulmala et al., 2011). This inventory of EC/OC is also provided by TNO and consists with the same spatial resolution and SNAP-code categorization as the AQMEII one. However, the point sources of EC in Germany were excluded due to their large uncertainties (Chen et al., 2016).

The Fire INventory from NCAR (FINN, Wiedinmyer et al., 2011), with the spatial resolution of 1 km and the temporal resolution of 1 hour, was also included. Biogenic emissions were presented by the Model of Emissions of Gases and Aerosols from Nature (MEGAN, Guenther et al., 2006). Dust emissions were not considered, due to the large uncertainty of the dust emission scheme in WRF-Chem (Saide et al., 2012). According to quartz-filter-based measurements (quartz-filter Type MK360, Munktell/Ahlstorn, Schweden) with high volume sampler DIGITEL DHA-80 (Walter RiemerMesstechnik, Germany), dust contributed less than 3% to the total particle mass concentration in Melpitz during the simulated period.

2.3 Observations

Measurements of HOPE-Campaign and the European Monitoring and Evaluation Programme (EMEP, http://www.emep.int) were adopted to validate the model results. In addition, radiosonde datasets

(http://www.weather.uwyo.edu/upperair/sounding.html) of Melpitz and the stations all over Europe were utilized to evaluate the modelled atmospheric vertical structures.

The Melpitz Obervatory is representative for the regional background of Central Europe (Spindler et al., 2012; Spindler et al., 2010; Poulain et al., 2011; Brüggemann and Spindler, 1999). The instruments that measure aerosol physical properties were operated under dry condition, as recommended by WMO-GAW and ACTRIS. A Dual Mobility Particle Size Spectrometer (TROPOS-type dual-SMPS, Birmili et al., 1999) combined with an Aerodynamic Particle Size Spectrometer (TSI APS Model 3321) were employed to measure the particle number size distribution (PNSD) ranging from 5 nm to 10 μm in diameter. Detailed information is given by Chen et al. (2016) and Heintzenberg et al. (1998). A MARGA system (Schaap et al., 2011; Thomas et al., 2009; ten Brink et al., 2007), continuously monitoring aerosol and gases in ambient air (Metrohm Applikon, Schiedam, The Netherlands), was operated downstream of a PM_{10} inlet. This instrument provided 1-hour data of secondary inorganic aerosols and gaseous counterparts. The high volume samplers DIGITEL DHA-80 (Walter RiemerMesstechnik, Germany), with sampling flow of about 30 $m^3 h^{-1}$, was operated for simultaneous daily samples of PM_{10} and PM_1 (Spindler et al., 2013). Information of aerosol chemical compositions, such as nitrate and sodium etc., in the coarse mode (PM_{1-10}) were obtained from the difference between the results of PM_{10} and PM_1. Additionally, filter sampler measurements with PM_{10} inlets (EMEP, 2014) at 3 coastal EMEP station near the SSA transportation pathway (Bilthoven, Vredepeel, and Kollumerwaad, see Fig. 1), were obtained from EBAS (http://ebas.nilu.no/), with a temporal resolution of 2 days.

3. Results & Discussion

3.1 Meteorology

During the HOPE-Campaign, continental air masses prevailed over the Northern Germany before September 15 (Fig. S3). On September 16, a low pressure trough began to dominate the North Sea, while a high pressure ridge dominated over the continent. A frontal system was clearly formed along the coast of the North Sea as could be seen in Fig. S4, accompanied by sharp wind shear and also high convective available potential energy (CAPE). Evidently, strong vertical mixing occurred in the coastal region, resulted in lifted SSA upward.

Meteorology simulated by WRF was evaluated with the near-ground measurements at Melpitz and radio-sounding measurements all over Europe. Both surface meteorology and the vertical structure of meteorological parameters were well captured by the model. Simulated temperature, relative humidity, wind speed and wind direction were in good agreement with measurements, with a correlation coefficients (R) of 0.94, 0.85, 0.86, and 0.86 respectively. The vertical gradient of potential temperature is an important indicator to measure the stability of the atmosphere. Fig. 2 shows a map of R values between the simulated and measured vertically-resolved potential temperature in planetary boundary layer (PBL, 0-3 km). High values of R were found at all stations, especially near Melpitz, Germany (R > 0.85) and the coast of North Sea (R > 0.95). Statistical results of comparisons between the simulation and Melpitz radio-sounding measurements are shown in Table S1. Several examples of vertical profiles are given in Chen et al. (2016). Simulated meteorological vertical structures were in good agreement with measurements in Melpitz. Corresponding, R values were 0.99, 0.96, 0.84 and 0.92 for potential temperature, wind speed, wind direction and water vapor mixing ratio, respectively. Therefore, the WRF simulations well reproduced the meteorological conditions for both ground level and vertical structure.

3.2 Aerosol physical and chemical properties

The modelled particle number size distribution (PNSD) and particle mass size distribution (PMSD) at Melpitz were compared with measurements (Fig. 3). The model significantly overestimated the concentration for the size bin 05-08 (625-10,000 nm). Since the meteorology was well reproduced by the model, it can be assumed

that the air movement was also reasonably simulated. As a consequence, there might be unrealistic sources of coarse particles leading to the overestimation.

The chemical compositions in PM_{1-10} of the DIGITEL measurements and simulation results at Melpitz are displayed in Fig. 4. The simulated particles composition for each size bin is shown in Fig. S2. Sea salt (Na^+) and

5   nitrate mass concentrations in PM_{1-10} were overestimated by factors of ~18 and ~2, respectively (see also Table 2 and 3). Particularly, the overestimation factors could reach up to ~20 and 3 respectively for Na^+ and nitrate in the period influenced by marine air masses (starting from September 16, see Fig. 4b). These results indicated that the overestimations in bin 05-08 were mainly caused by SSA and nitrate.

3.3 Sea salt emission and the transport

10 For the sea salt event studied here, the abrupt SSA event was found to be emitted over the North Sea and overall overestimated in the coastal and continental regions during September 16-20, as shown in Fig. 5. Here we used sodium (Na^+) as an indicator of SSA (Neumann et al., 2016; Gustafsson and Franzén, 2000), since chloride (Cl^-) could be depleted due to nitrate formation (Schaap et al., 2011; Seinfeld, 2006). Marine air masses arrived at three coastal stations (Bilthoven, Vredepeel, and Kollumerwaad, see Fig. 1) first, and then went

15 further inland along with the low-pressure trough system. The Na^+ concentration peaked on September 16 for the coastal stations, and about 1 day later for Melpitz (Fig. 5).

As shown in Fig. 5 the variance/trend of Na^+ concentrations can be captured by the model, with the correlation coefficient (R) of 0.95, 0.81, 0.92 and 0.89 for Melpitz, Bilthoven, Kollumerwaard and Vredepeel respectively. The transport mechanism was well captured by the model in general. However, SSA mass concentrations were

20 overestimated by about 20 times in Melpitz and around 9, 13 and 8 times respectively for the coastal stations of Bilthoven, Kollumerwaard and Vredepeel. This implies that the emission scheme of SSA may be overestimated by a factor of 8-20. The overestimation was consistent with previous modeling studies using WRF-Chem: in the Southeast Pacific ocean (Saide et al., 2012), in the coast region of California USA (Saide et al., 2013), over Europe (Nordmann et al., 2014; Zhang et al., 2013) and over the cold waters of the Southern, North Pacific and

25 North Atlantic Oceans (Jaeglé et al., 2011). The parameterization scheme (Gong, 2003) describes SSA emission as a function of wind speed at 10 meter above the ground. The uncertainties of this scheme may be attributable to the missing of parameters, such as sea surface temperature (Soares et al., 2016; Grythe et al., 2014; Jaeglé et al., 2011), salinity (Soares et al., 2016; Neumann et al., 2016) and wave data (Ovadnevaite et al., 2014; Jaeglé et al., 2011). The missing of proper droplet generation processes might be another source of the uncertainties

30 (Neumann et al., 2016).

After been emitted over North Sea, the SSA might experience chemical degradation (such as Cl^- depletion) and dry/wet deposition when transported over continental area. Generally, SSA is mostly in coarse mode with lifetime shorter than 2 days in the continental boundary layer, whereas about 1 week in free troposphere (Croft et al., 2014; Petzold and Kärcher, 2012; Jaenicke, 1980). According to the simulation results, the wind speed at

35 10 meter above the ground was about 2-3 ms^{-1} with the direction from the coast to Melpitz (Fig. 1). It took therefore about 1.5-2 days for SSA to be transported to Melpitz (~400 km away from coast). The result (Fig. S5) from Deposition-Lifetime Concept Model (Chen et al., 2016; Croft et al., 2014) indicated that on average only about 10-35% of SSA could be transported to Melpitz through the surface pathway. Whereas, according to the observed SSA peaks (Fig. 5), about 30-40% of SSA mass concentration was actually transported to the inland

40 (Melpitz) comparing to the coastal regions. The observed transport efficiency was about 1.6 times of the expected value. So, the transport mechanism of the SSA to the inland (Melpitz) will be discussed with the aid of a model simulation, despite the overestimation in the WRF-Chem SSA emission scheme. As demonstrated in Fig. 6, during nighttime, the warmer sea surface resulted in a higher planetary boundary layer (PBL, black dash lines in Fig. 6) than that over the continent (Dacre et al., 2007; Lu and Turco, 1995, 1994). Due to the difference of

45 thermodynamic structure between continental and marine area, there is often a sharp gradient of PBL height

Atmospheric
Chemistry
and Physics

Open Access

Discussions

EGU

over the coastal region (Fig. 6), which could serve as an "aloft bridge" connecting the marine PBL and continental free troposphere (Dacre et al., 2007; Lu and Turco, 1995, 1994). In the early morning of September 16, SSA was emitted near the surface layer of North Sea and lifted upward by convective mixing and turbulence (Fig. 6a). According to the simulation result (Fig. 6), about 70% of SSA was able to penetrate the marine PBL and

5   was injected into continent free troposphere through the "aloft bridge". In the free troposphere, SSA has a much longer life time and faster transportation than in the PBL. Therefore, about 70-85% of SSA (Fig. S5) could be carried further towards inland in free troposphere, and arrived the Melpitz region in the early morning of September 17 (Fig. 6b). Then the downward draft, resulted from high-pressure ridge, brought the lofted SSA back into the surface layer (Fig. 6b).

10   **3.4 Influence of sea salt on nitrate simulation**

As discussed above, the over production of SSA from the WRF-Chem SSA emission scheme will leads to an 8-20 times overestimation of the primary sea salt mass concentration. However, its influence on the simulation is not only on the primary SSA, but also on promoting the formation of secondary inorganic aerosol (SIA), such as nitrate (Neumann et al., 2016; Seinfeld, 2006). The gas phase nitric acid (HNO_3) can be produced with the

15   oxidization of NOx. Part of HNO_3 will participate in the partitioning processes and form particulate nitrate. In MOSAIC aerosol scheme (Zaveri et al., 2008), one partitioning process between gas phase and solid phase is the equilibrium reaction with ammonia (NH_3) and the formation of ammonium nitrate. Another one is the irreversibly reaction with SSA (NaCl) and the formation of sodium nitrate with depletion of chloride. Ammonium nitrate is semi-volatile and can turn back to the gas phase precursors, while sodium nitrate is

20   thermodynamically stable (Schaap et al., 2011). The participation of SSA might facilitate the partitioning process of nitrate. For the deliquescent aerosol particles at high RH, the ionization equilibrium and the Kelvin Effect are also taken into consideration in MOSAIC. More detailed descriptions are given in Zaveri et al. (2008).

Comparisons of nitrate and its precursors between the simulation results and the MARGA measurements at Melpitz are shown in Fig. 7. Overall, nitrate in the size range of PM_{10} was overestimated by the model, with an

25   average factor of ~5 (Table 2). Either it could result from inaccurate emission of precursors or an improper chemical pathway. Assuming that the chemical mechanism is correctly described in the model, the same concentration of gaseous precursors (NOx and ammonia) should produce the same concentration of nitrate in the model and observation. The location of the data dots (Fig. 7a) may be shifted due to the uncertainty of precursors emissions, but the nitrate mass concentration is always expected to be consistent with the observed

30   concentration in Fig. 7b. The difference between Fig. 7a and Fig. 7b indicates that in addition to an overestimation caused by overestimated NH3 emission (see also Table 2), improper chemical pathway also contributed to the nitrate overestimation. Since the simulated nitrate mass concentrations (Fig. 7a) were still much higher than the observed one (Fig. 7b), even though where had the same mass concentrations of precursors.

35   In order to quantify the influence of NaCl on the nitrate partitioning, a sensitive study was implemented with only 5% of SSA emission (R-CASE). The comparisons between the full SSA emission case (F-CASE, 100% SSA emission) and R-CASE are shown in Table 2 and Table 3. The simulated NOx concentrations were in good agreements with measurements, but total ammonia was overestimated by a factor of ~2 in both cases (Table 2), which may stem from the uncertainty of ammonia emission inventory. The simulation of SSA (Na^+) was

40   significantly improved after reducing SSA emission, with a factor of 1.09 and R value of 0.94 for size range of 1-10 μm at Melpitz (Table 3). Also, results at coastal stations were not overestimated in the R-CASE. However, NOx and total ammonia concentrations results of these two cases were not significantly changed (Table 2). Therefore, the difference of nitrate between the F-CASE and the R-CASE should mainly arise from the influence of the SSA concentrations. The overestimation factor of nitrate at Melpitz dramatically decreased from 2.1 to

45   0.73 in coarse mode (PM_{1-10}, see Table 2).

The participation of SSA changes the partitioning processes of nitrate. In order to quantify this effect, the nitrate partitioning fraction (PF_nitrate) was analyzed for coarse mode (PM$_{1-10}$) and fine mode (PM$_1$) particles. The definition of PF_nitrate for coarse/fine mode is shown in Eq.1.

$$PF\_nitrate_{coarse/fine} = \frac{[NO_3^-]_{coarse/fine}}{[NO_3^-]_{coarse/fine} + [HNO_3]}, \tag{1}$$

5

where [NO$_3^-$]$_{coarse/fine}$ is the coarse/fine mode particulate nitrate mass concentration, [HNO$_3$] is the nitric acid mass concentration.

The comparisons of the PF_nitrate probability density function (PF_nitrate-PDF) between the F-CASE and the R-CASE are shown in Fig. 8, respectively for fine mode (PM$_1$) and coarse mode (PM$_{1-10}$) particles during the marine
10   period (Na$^+$>1.8 µg/m^3 in F-CASE). Note that PF_nitrate derived from MARGA observations should not be directly compared with the simulated one. Since MARGA measurements were only available for the size range of PM$_{10}$, and high uncertainty of the HNO$_3$ measurement due to its sticky property; also there was uncertainty of the precursors emissions in the model. In this study, the R-CASE had a much more reasonable SSA prediction (within a factor of ~1 at Melpitz) than the F-CASE; therefore, the simulated values of PF_nitrate from R-CASE
15   were used as the reference. Considering that most of the SSA was emitted as coarse mode particles (about 88% in both filter measurement and simulation on September 17, 2013 at Melpitz), the PF_nitrate results for coarse mode particles should be more representative for the influence of SSA on particulate nitrate formation, also more sensitive to the change of the SSA emission. As shown in Fig. 8a and Fig. 8b, the median value of coarse mode PF_nitrate was about 0.75 in R-CASE broadly spreading from ~0.2 to 1, and it increased to 0.96 in F-CASE
20   with a much narrowed distribution. This indicated that the participation of SSA increased the coarse mode nitrate partitioning fraction by ~0.2, which contributed to about 140% overestimation of the coarse mode nitrate (Table 2). In this case study, SSA was highly overestimated by the model in F-CASE and the overestimated amount was transported to the surface layer at Melpitz, which means more SSA participated in the nitrate partitioning process and formed stable sodium nitrate and accumulated in the coarse mode.

25   While for the fine mode nitrate, the PF_nitrate of fine mode was insensitive to SSA emission (Fig. 8), indicating that in our case the overestimation of SSA emission is mainly in the coarse mode. Although the fine mode PF_nitrate had no significant difference between R-CASE and F-CASE simulations (Fig. 8c and Fig. 8d), the fine mode nitrate mass concentration was reduced by ~20% in F-CASE due to the consumption of precursors by the coarse mode nitrate formation. Therefore, the total nitrate mass concentrations in size range of PM$_{10}$ were
30   similar between R-CASE and F-CASE (Table 2).

In general, the overestimation of SSA emission scheme has a significant influence on the particulate nitrate simulation in both the coarse mode (directly) and the fine mode (indirectly). In this case study, the overestimation of SSA in the F-CASE made the coarse mode nitrate partitioning fraction overestimated by ~0.2. The increasing of consumption of precursors in the coarse mode nitrate formation might slow down the
35   formation of nitrate in the fine mode. The particle number/mass size distribution (PNSD/PMSD) was thus altered due to these influences.

4 Conclusions

In order to investigate the SSA emission and transportation in Central Europe and its influence on nitrate simulation, the WRF-Chem model was used to simulate physical and chemical aerosol properties during HOPE-
40   Campaign, September 10-20, 2013, at Melpitz. The simulated meteorological variables, vertical thermal

stratification, and near-ground level particle number size distribution were validated by observations. The ground meteorology and vertical thermal stratification were well captured by the model. The coarse mode particles were however significantly overestimated, due to uncertainty of the SSA emission scheme and coarse mode nitrate.

5   SSA mass concentrations were evaluated at 4 EMEP stations, including 1 continental inland station (Melpitz) and 3 coastal stations (Bilthoven, Kollumerwaard and Vredepeel). The variations of SSA mass concentrations were well captured by the model, despite that the concentrations were overestimated by a factor of 8-20 due to the overestimation in WRF-Chem SSA emission scheme. In addition to the wind speed at 10 meter above the ground, more parameters, such as sea surface temperature, salinity and wave data, might need to be considered into the SSA emission scheme to reduce its uncertainty. Transport of SSA from North Sea to inland
10   was analyzed in detail. Due to different nighttime PBL structure over continent and marine region, an "aloft bridge" between the marine PBL and continental free troposphere was formed over the coastal area. The overestimated SSA released from the North Sea was mixed up and injected into the continental free troposphere, and participated in the long-range transport, because the lifetime of aerosols can be about 5 times longer in free troposphere than in the PBL. This injected SSA was transported over Melpitz and later on mixed
15   downward to the surface by the downdraft and the turbulence of fully developed PBL on September 17, 2013. The overestimation of SSA emission combined with the "aloft bridge" transport process together made the SSA overestimated by a factor of 20 at Melpitz.

The overestimation of SSA emission is not only a problem of primary SSA itself, it may also cause the significant
20   uncertainty of particulate nitrate simulation. As described in Fig. 9, more nitrate and precursors can be locked in the sodium nitrate which is thermodynamically stable, due to the participation of more SSA in the nitrate partitioning process. Since most of the SSA was emitted as coarse mode particles, nitrate partitioning fraction of coarse mode was overestimated by ~0.2 when the SSA mass concentration was highly overestimated. This contributed about 140% overestimation of the coarse mode nitrate. The nitrate partitioning fraction of fine
25   mode was insensitive to the SSA emission. However, the increasing consumption of the gas-phase precursors, resulted from coarse mode nitrate formation with participation of SSA, may slow down the formation of fine mode nitrate.

In this paper, the transport process of SSA from the North Sea to Central Europe was demonstrated in detail, the emission of SSA was evaluated and the influence of SSA on particulate nitrate simulation was quantitatively
30   analyzed. The uncertainty of SSA emission is not only the matter of primary aerosol, but also has significant influence on the formation of secondary inorganic aerosol (like nitrate). It will change the heterogeneous reaction process and the pathway from gas phase precursors to particulate phase. Later on, these changes will alter the physical and chemical aerosol properties, e.g. particle number/mass size distribution and hygroscopicity, which are crucial for climate change evaluation. Furthermore, the direct and indirect radiative
35   forcing evaluation will also be influenced. The "aloft bridge" transport mechanism, as described in this paper, makes these influences of SSA not only along the coastal region, but also in a broader scope reaching as far as 400 km from coast. Meanwhile, the outflow of continental air mass which transport NOx to the ocean region (Fig. S1), where these influences of SSA on nitrate may also be significant.

References:

Archer-Nicholls, S., Lowe, D., Utembe, S., Allan, J., Zaveri, R. A., Fast, J. D., Hodnebrog, Ø., Denier van der Gon, H., and McFiggans, G.: Gaseous chemistry and aerosol mechanism developments for version 3.5.1 of the online regional model, WRF-Chem, Geosci. Model Dev., 7, 2557-2579, 10.5194/gmd-7-2557-2014, 2014.

5 Athanasopoulou, E., Tombrou, M., Pandis, S. N., and Russell, A. G.: The role of sea-salt emissions and heterogeneous chemistry in the air quality of polluted coastal areas, Atmos. Chem. Phys., 8, 5755-5769, 10.5194/acp-8-5755-2008, 2008.

Barnard, J. C., Chapman, E. G., Fast, J. D., Schmelzer, J. R., Slusser, J. R., and Shetter, R. E.: An evaluation of the FAST-J photolysis algorithm for predicting nitrogen dioxide photolysis rates under clear and cloudy sky
10 conditions, Atmospheric Environment, 38, 3393-3403, http://dx.doi.org/10.1016/j.atmosenv.2004.03.034, 2004.

Binkowski, F. S., and Shankar, U.: The Regional Particulate Matter Model: 1. Model description and preliminary results, Journal of Geophysical Research: Atmospheres, 100, 26191-26209, 10.1029/95JD02093, 1995.

Birmili, W., Stratmann, F., and Wiedensohler, A.: Design of a DMA-based size spectrometer for a large particle size range and stable operation, Journal of Aerosol Science, 30, 549-553, http://dx.doi.org/10.1016/S0021-
15 8502(98)00047-0, 1999.

Brüggemann, E., and Spindler, G.: Wet and dry deposition of sulphur at the site Melpitz in East Germany, Water Air Soil Pollut 109, 81-99, 1999.

Chapman, E. G., Gustafson Jr, W. I., Easter, R. C., Barnard, J. C., Ghan, S. J., Pekour, M. S., and Fast, J. D.: Coupling aerosol-cloud-radiative processes in the WRF-Chem model: Investigating the radiative impact of
20 elevated point sources, Atmos. Chem. Phys., 9, 945-964, 10.5194/acp-9-945-2009, 2009.

Chen, Y., Zhao, C., Zhang, Q., Deng, Z. Z., Huang, M. Y., and Ma, X. C.: Aircraft study of mountain chimney effect of Beijing, china, Journal of Geophysical Research: Atmospheres, 114, 10.1029/2008JD010610, 2009.

Chen, Y., Cheng, Y. F., Nordmann, S., Birmili, W., Denier van der Gon, H. A. C., Ma, N., Wolke, R., Wehner, B., Sun, J., Spindler, G., Mu, Q., Pöschl, U., Su, H., and Wiedensohler, A.: Evaluation of the size segregation of elemental
25 carbon (EC) emission in Europe: influence on the simulation of EC long-range transportation, Atmos. Chem. Phys., 16, 1823-1835, 10.5194/acp-16-1823-2016, 2016.

Croft, B., Pierce, J. R., and Martin, R. V.: Interpreting aerosol lifetimes using the GEOS-Chem model and constraints from radionuclide measurements, Atmos. Chem. Phys., 14, 4313–4325, doi:10.5194/acp-14-4313-2014, 2014.

30 Dacre, H. F., Gray, S. L., and Belcher, S. E.: A case study of boundary layer ventilation by convection and coastal processes, Journal of Geophysical Research: Atmospheres, 112, 10.1029/2006JD007984, 2007.

de Leeuw, G., Neele, F. P., Hill, M., Smith, M. H., and Vignati, E.: Production of sea spray aerosol in the surf zone, Journal of Geophysical Research: Atmospheres, 105, 29397-29409, 10.1029/2000JD900549, 2000.

de Leeuw, G., Andreas, E. L., Anguelova, M. D., Fairall, C. W., Lewis, E. R., O'Dowd, C., Schulz, M., and Schwartz,
35 S. E.: Production flux of sea spray aerosol, Reviews of Geophysics, 49, 10.1029/2010RG000349, 2011.

EMEP: EMEP Manual for Sampling and Analysis, EMEP, available at: http://www.nilu.no/projects/ccc/manual/index.html (last access: November 30th, 2015), 2014.

Atmospheric
Chemistry
and Physics
Discussions

Open Access

EGU

Fast, J. D., Gustafson, W. I., Easter, R. C., Zaveri, R. A., Barnard, J. C., Chapman, E. G., Grell, G. A., and Peckham, S. E.: Evolution of ozone, particulates, and aerosol direct radiative forcing in the vicinity of Houston using a fully coupled meteorology-chemistry-aerosol model, Journal of Geophysical Research: Atmospheres, 111, 10.1029/2005JD006721, 2006.

5   Fountoukis, C., and Nenes, A.: ISORROPIA II: a computationally efficient thermodynamic equilibrium model for $K^+–Ca^{2+}–Mg^{2+}–NH_4^+–Na^+–SO_4^{2−}–NO_3^−–Cl^−–H_2O$ aerosols, Atmos. Chem. Phys., 7, 4639-4659, 10.5194/acp-7-4639-2007, 2007.

Gong, S. L.: A parameterization of sea-salt aerosol source function for sub- and super-micron particles, Global Biogeochemical Cycles, 17, 10.1029/2003GB002079, 2003.

10   Grell, G. A., Peckham, S. E., Schmitz, R., McKeen, S. A., Frost, G., Skamarock, W. C., and Eder, B.: Fully coupled "online" chemistry within the WRF model, Atmospheric Environment, 39, 6957-6975, http://dx.doi.org/10.1016/j.atmosenv.2005.04.027, 2005.

Grythe, H., Ström, J., Krejci, R., Quinn, P., and Stohl, A.: A review of sea-spray aerosol source functions using a large global set of sea salt aerosol concentration measurements, Atmos. Chem. Phys., 14, 1277-1297, 15   10.5194/acp-14-1277-2014, 2014.

Guenther, A., Karl, T., Harley, P., Wiedinmyer, C., Palmer, P. I., and Geron, C.: Estimates of global terrestrial isoprene emissions using MEGAN (Model of Emissions of Gases and Aerosols from Nature), Atmos. Chem. Phys., 6, 3181-3210, 10.5194/acp-6-3181-2006, 2006.

Gustafsson, M. E. R., and Franzén, L. G.: Inland transport of marine aerosols in southern Sweden, Atmospheric 20   Environment, 34, 313-325, http://dx.doi.org/10.1016/S1352-2310(99)00198-3, 2000.

Heintzenberg, J., Müller, K., Birmili, W., Spindler, G., and Wiedensohler, A.: Mass-related aerosol properties over the Leipzig Basin, Journal of Geophysical Research: Atmospheres, 103, 13125-13135, 10.1029/98JD00922, 1998.

Im, U.: Impact of sea-salt emissions on the model performance and aerosol chemical composition and deposition in the East Mediterranean coastal regions, Atmospheric Environment, 75, 329-340, 25   http://dx.doi.org/10.1016/j.atmosenv.2013.04.034, 2013.

IPCC, A. R.: Climate Change 2013: The Physical Science Basis. Contribution of Working Group I to the Fifth Assessment Report of the Intergovernmental Panel on Climate Change, Report, Cambridge University Press, New York,, 2013.

Jaeglé, L., Quinn, P. K., Bates, T. S., Alexander, B., and Lin, J. T.: Global distribution of sea salt aerosols: new 30   constraints from in situ and remote sensing observations, Atmos. Chem. Phys., 11, 3137-3157, 10.5194/acp-11-3137-2011, 2011.

Jaenicke, R.: Atmospheric aerosols and global climate, Journal of Aerosol Sciences, 11, 577-588, 1980.

Kulmala, M., Asmi, A., Lappalainen, H. K., Baltensperger, U., Brenguier, J. L., Facchini, M. C., Hansson, H. C., Hov, Ø., O'Dowd, C. D., Pöschl, U., Wiedensohler, A., Boers, R., Boucher, O., de Leeuw, G., Denier van der Gon, H. A. 35   C., Feichter, J., Krejci, R., Laj, P., Lihavainen, H., Lohmann, U., McFiggans, G., Mentel, T., Pilinis, C., Riipinen, I., Schulz, M., Stohl, A., Swietlicki, E., Vignati, E., Alves, C., Amann, M., Ammann, M., Arabas, S., Artaxo, P., Baars, H., Beddows, D. C. S., Bergström, R., Beukes, J. P., Bilde, M., Burkhart, J. F., Canonaco, F., Clegg, S. L., Coe, H., Crumeyrolle, S., D'Anna, B., Decesari, S., Gilardoni, S., Fischer, M., Fjaeraa, A. M., Fountoukis, C., George, C., Gomes, L., Halloran, P., Hamburger, T., Harrison, R. M., Herrmann, H., Hoffmann, T., Hoose, C., Hu, M., 40   Hyvärinen, A., Hõrrak, U., Iinuma, Y., Iversen, T., Josipovic, M., Kanakidou, M., Kiendler-Scharr, A., Kirkevåg, A.,

Kiss, G., Klimont, Z., Kolmonen, P., Komppula, M., Kristjánsson, J. E., Laakso, L., Laaksonen, A., Labonnote, L., Lanz, V. A., Lehtinen, K. E. J., Rizzo, L. V., Makkonen, R., Manninen, H. E., McMeeking, G., Merikanto, J., Minikin, A., Mirme, S., Morgan, W. T., Nemitz, E., O'Donnell, D., Panwar, T. S., Pawlowska, H., Petzold, A., Pienaar, J. J., Pio, C., Plass-Duelmer, C., Prévôt, A. S. H., Pryor, S., Reddington, C. L., Roberts, G., Rosenfeld, D., Schwarz, J.,

5 Seland, Ø., Sellegri, K., Shen, X. J., Shiraiwa, M., Siebert, H., Sierau, B., Simpson, D., Sun, J. Y., Topping, D., Tunved, P., Vaattovaara, P., Vakkari, V., Veefkind, J. P., Visschedijk, A., Vuollekoski, H., Vuolo, R., Wehner, B., Wildt, J., Woodward, S., Worsnop, D. R., van Zadelhoff, G. J., Zardini, A. A., Zhang, K., van Zyl, P. G., Kerminen, V. M., S Carslaw, K., and Pandis, S. N.: General overview: European Integrated project on Aerosol Cloud Climate and Air Quality interactions (EUCAARI) – integrating aerosol research from nano to global scales, Atmos.

10 Chem. Phys., 11, 13061-13143, 10.5194/acp-11-13061-2011, 2011.

Lewis, E. R. S., S. E.: Sea Salt Aerosol Production: Mechanisms, Methods, Measurements and Models - A Critical Review, AGU, Washington, D. C., 152, 29711, doi:10.1029/GM152, 2004.

Liu, Y., Zhang, S., Fan, Q., Wu, D., Chan, P., Wang, X., Fan, S., Feng, Y., and Hong, Y.: Accessing the Impact of Sea-Salt Emissions on Aerosol Chemical Formation and Deposition over Pearl River Delta, China, Aerosol Air Qual.

15 Res., 15, 2232–2245, 10.4209/aaqr.2015.02.0127, 2015.

Lu, R., and Turco, R. P.: Air Pollutant Transport in a Coastal Environment. Part I: Two-Dimensional Simulations of Sea-Breeze and Mountain Effects, Journal of the Atmospheric Sciences, 51, 2285-2308, 10.1175/1520-0469(1994)051<2285:APTIAC>2.0.CO;2, 1994.

Lu, R., and Turco, R. P.: Air pollutant transport in a coastal environment—II. Three-dimensional simulations over

20 Los Angeles basin, Atmospheric Environment, 29, 1499-1518, http://dx.doi.org/10.1016/1352-2310(95)00015-Q, 1995.

Mårtensson, E. M., Tunved, P., Korhonen, H., and Nilsson, E. D.: The role of sea-salt emissions in controlling the marine Aitken and accumulation mode aerosol: a model study, Tellus B, 62, 10.3402/tellusb.v62i4.16552, 2010.

Meng, Z., and Seinfeld, J. H.: Time scales to achieve atmospheric gas-aerosol equilibrium for volatile species,

25 Atmospheric Environment, 30, 2889-2900, http://dx.doi.org/10.1016/1352-2310(95)00493-9, 1996.

Monahan, E. C., Spiel, D. E., and Davidson, K. L.: A model of marine aerosol generation via whitecaps and wave disruption, in: Oceanic Whitecaps edited by: Monahan, E. and Niocaill, G. M.,, D. Reidel, Norwell, Mass, 167-174, 1986.

Monahan, E. C.: Coastal Aerosol Workshop Proceedings, edited by: Goroch, A. K. and Geernaert, G. L., Rep.

30 NRL/MR/7542-95-7219, 138 pp., Nav. Res. Lab., Monterey, Calif., 1995.

Neumann, D., Matthias, V., Bieser, J., Aulinger, A., and Quante, M.: Sensitivity of modeled atmospheric nitrogen species and nitrogen deposition to variations in sea salt emissions in the North Sea and Baltic Sea regions, Atmos. Chem. Phys., 16, 2921-2942, 10.5194/acp-16-2921-2016, 2016.

Nordmann, S., Cheng, Y. F., Carmichael, G. R., Yu, M., Denier van der Gon, H. A. C., Zhang, Q., Saide, P. E., Pöschl,

35 U., Su, H., Birmili, W., and Wiedensohler, A.: Atmospheric black carbon and warming effects influenced by the source and absorption enhancement in central Europe, Atmos. Chem. Phys., 14, 12683-12699, 10.5194/acp-14-12683-2014, 2014.

Ovadnevaite, J., Manders, A., de Leeuw, G., Ceburnis, D., Monahan, C., Partanen, A. I., Korhonen, H., and O'Dowd, C. D.: A sea spray aerosol flux parameterization encapsulating wave state, Atmos. Chem. Phys., 14,

40 1837-1852, 10.5194/acp-14-1837-2014, 2014.

Atmospheric
Chemistry
and Physics
Discussions

Open Access

EGU

Pakkanen, T. A., Hillamo, R. E., Aurela, M., Andersen, H. V., Grundahl, L., Ferm, M., Persson, K., Karlsson, V., Reissell, A., Røyset, O., Fløisand, I., Oyola, P., and Ganko, T.: Nordic intercomparison for measurement of major atmospheric nitrogen species, Journal of Aerosol Science, 30, 247-263, http://dx.doi.org/10.1016/S0021-8502(98)00039-1, 1999.

5   Petzold, A., and Kärcher, B.: Aerosols in the Atmosphere, in: Atmospheric Physics, edited by: Schumann, U., Research Topics in Aerospace, Springer Berlin Heidelberg, 37-53, DOI: 10.1007/978-3-642-30183-4_3, 2012.

Pope, C. A., Ezzati, M., and Dockery, D. W.: Fine-particulate air pollution and life expectancy in the united states, N. Engl. J. Med., 360, 376–386, 2009.

Poulain, L., Spindler, G., Birmili, W., Plass-Dülmer, C., Wiedensohler, A., and Herrmann, H.: Seasonal and diurnal
10   variations of particulate nitrate and organic matter at the IfT research station Melpitz, Atmos. Chem. Phys., 11, 12579-12599, 2011.

Pouliot, G., Pierce, T., Denier van der Gon, H., Schaap, M., Moran, M., and Nopmongcol, U.: Comparing emission inventories and model-ready emission datasets between Europe and North America for the AQMEII project, Atmospheric Environment, 53, 4-14, http://dx.doi.org/10.1016/j.atmosenv.2011.12.041, 2012.

15   Saide, P. E., Spak, S. N., Carmichael, G. R., Mena-Carrasco, M. A., Yang, Q., Howell, S., Leon, D. C., Snider, J. R., Bandy, A. R., Collett, J. L., Benedict, K. B., de Szoeke, S. P., Hawkins, L. N., Allen, G., Crawford, I., Crosier, J., and Springston, S. R.: Evaluating WRF-Chem aerosol indirect effects in Southeast Pacific marine stratocumulus during VOCALS-REx, Atmos. Chem. Phys., 12, 3045-3064, 10.5194/acp-12-3045-2012, 2012.

Saide, P. E., Carmichael, G. R., Liu, Z., Schwartz, C. S., Lin, H. C., da Silva, A. M., and Hyer, E.: Aerosol optical
20   depth assimilation for a size-resolved sectional model: impacts of observationally constrained, multi-wavelength and fine mode retrievals on regional scale analyses and forecasts, Atmos. Chem. Phys., 13, 10425-10444, 10.5194/acp-13-10425-2013, 2013.

Schaap, M., Müller, K., and ten Brink, H. M.: Constructing the European aerosol nitrate concentration field from quality analysed data, Atmospheric Environment, 36, 1323-1335, http://dx.doi.org/10.1016/S1352-
25   2310(01)00556-8, 2002.

Schaap, M., Otjes, R. P., and Weijers, E. P.: Illustrating the benefit of using hourly monitoring data on secondary inorganic aerosol and its precursors for model evaluation, Atmos. Chem. Phys., 11, 11041-11053, 10.5194/acp-11-11041-2011, 2011.

Seinfeld, J. H.: Atmospheric Chemistry and Physics -- From Air Pollution to Climate Change, A Wiley-Interscience
30   Publication, 2006.

Soares, J., Sofiev, M., Geels, C., Christensen, J. H., Andersson, C., Tsyro, S., and Langner, J.: Impact of climate change on the production and transport of sea salt aerosol on European seas, Atmos. Chem. Phys. Discuss., 2016, 1-52, 10.5194/acp-2015-1056, 2016.

Spindler, G., Brüggemann, E., Gnauk, T., Grüner, A., Müller, K., and Herrmann, H.: A four-year size-segregated
35   characterization study of particles PM10, PM2.5 and PM1 depending on air mass origin at Melpitz, Atmospheric Environment, 44, 164-173, 2010.

Spindler, G., Gnauk, T., Grüner, A., Iinuma, Y., Müller, K., Scheinhardt, S., and Herrmann, H.: Size-segregated characterization of PM10 at the EMEP site Melpitz (Germany) using a five-stage impactor: a six year study, J Atmos Chem, 69, 127-157, 10.1007/s10874-012-9233-6, 2012.

Atmospheric
Chemistry
and Physics
Discussions

Spindler, G., Grüner, A., Müller, K., Schlimper, S., and Herrmann, H.: Long-term size-segregated particle (PM10, PM2.5, PM1) characterization study at Melpitz -- influence of air mass inflow, weather conditions and season, J Atmos Chem, 70, 165-195, 10.1007/s10874-013-9263-8, 2013.

5   ten Brink, H., Otjes, R., Jongejan, P., and Slanina, S.: An instrument for semi-continuous monitoring of the size-distribution of nitrate, ammonium, sulphate and chloride in aerosol, Atmospheric Environment, 41, 2768-2779, http://dx.doi.org/10.1016/j.atmosenv.2006.11.041, 2007.

ten Brink, H. M., Kruisz, C., Kos, G. P. A., and Berner, A.: Composition/size of the light-scattering aerosol in the Netherlands, Atmospheric Environment, 31, 3955-3962, http://dx.doi.org/10.1016/S1352-2310(97)00232-X, 1997.

10   Thomas, R. M., Trebs, I., Otjes, R., Jongejan, P. A. C., Brink, H. t., Phillips, G., Kortner, M., Meixner, F. X., and Nemitz, E.: An Automated Analyzer to Measure Surface-Atmosphere Exchange Fluxes of Water Soluble Inorganic Aerosol Compounds and Reactive Trace Gases, Environmental Science & Technology, 43, 1412-1418, 10.1021/es8019403, 2009.

Visschedijk, A., and Denier van der Gon, H.: EUCAARI deliverable : Pan-European Carbonaceous aerosol
15   inventory, Report, TNO Built Environment and Geosciences, D42, Utrecht, Netherlands, 2008.

Wiedinmyer, C., Akagi, S. K., Yokelson, R. J., Emmons, L. K., Al-Saadi, J. A., Orlando, J. J., and Soja, A. J.: The Fire INventory from NCAR (FINN): a high resolution global model to estimate the emissions from open burning, Geosci. Model Dev., 4, 625-641, 10.5194/gmd-4-625-2011, 2011.

Wild, O., Zhu, X., and Prather, M. J.: Fast-J: Accurate Simulation of In- and Below-Cloud Photolysis in
20   Tropospheric Chemical Models, J. Atmos. Chem., 37, 245-282, 2000.

Wolke, R., Schröder, W., Schrödner, R., and Renner, E.: Influence of grid resolution and meteorological forcing on simulated European air quality: A sensitivity study with the modeling system COSMO–MUSCAT, Atmospheric Environment, 53, 110-130, http://dx.doi.org/10.1016/j.atmosenv.2012.02.085, 2012.

Woodcock, A. H., Blanchard, D. C., and Rooth, C. G. H.: Saltinduced convection and clouds, J. Atmos. Sci., 20,
25   159-169, 1963.

Yang, Q., W. I. Gustafson, J., Fast, J. D., Wang, H., Easter, R. C., Morrison, H., Lee, Y. N., Chapman, E. G., Spak, S. N., and Mena-Carrasco, M. A.: Assessing regional scale predictions of aerosols, marine stratocumulus, and their interactions during VOCALS-REx using WRF-Chem, Atmos. Chem. Phys., 11, 11951-11975, 10.5194/acp-11-11951-2011, 2011.

30   Zaveri, R. A., and Peters, L. K.: A new lumped structure photochemical mechanism for large-scale applications, J. Geophys. Res., 104, 30387-30415, 1999.

Zaveri, R. A., Easter, R. C., Fast, J. D., and Peters, L. K.: Model for Simulating Aerosol Interactions and Chemistry (MOSAIC), Journal of Geophysical Research: Atmospheres, 113, 10.1029/2007JD008782, 2008.

Zhang, Y., Sartelet, K., Zhu, S., Wang, W., Wu, S. Y., Zhang, X., Wang, K., Tran, P., Seigneur, C., and Wang, Z. F.:
35   Application of WRF/Chem-MADRID and WRF/Polyphemus in Europe – Part 2: Evaluation of chemical concentrations and sensitivity simulations, Atmos. Chem. Phys., 13, 6845-6875, 10.5194/acp-13-6845-2013, 2013.

Table 1. Configurations of WRF-Chem

Physics	WRF options
Micro physics	(Lin, 1983) scheme
Boundary layer	YSU (Hong, 2006)
Surface	Rapid Update Cycle (RUC) land surface model
Shortwave radiation	Goddard shortwave (Chou, 1998)
Longwave radiation	New Goddard scheme
Cumulus	Grell 3D
Urban	3-category UCM
Chemistry and Aerosol	**Chem options**
Aerosol module	MOSAIC with 8 bins
Gas-phase mechanism	CBMZ
Photolytic rate	Fast-J photolysis scheme
Sea salt emission	Gong (2003) scheme

Atmospheric
Chemistry
and Physics
Discussions

Open Access

Table 2. Comparison of WRF-Chem results with Melpitz near-ground filter measurements

	F-CASE (100% SSA emission) Factor (R)	R-CASE (5% SSA emission) Factor (R)
NOx	0.98 (0.73)	0.98 (0.73)
Total Ammonia	2.12 (0.59)	2.21 (0.60)
Nitrate in PM_{10}	5.09 (0.76)	4.97 (0.72)
Nitrate in PM_{1-10}	2.10 (0.31)	0.73 (0.33)

Atmospheric
Chemistry
and Physics
Discussions

Table 3. Comparison of WRF-Chem modeled Na^+ mass concentration results with 4 EMEP stations measurements

Stations	F-CASE (100% SSA emission) Factor (R) of Na	R-CASE (5% SSA emission) Factor (R) of Na
Melpitz (PM_{10})	20.10 (0.95)	1.25 (0.94)
Melpitz (PM_{1-10})	18.10 (0.94)	1.09 (0.94)
Bilthoven (PM_{10})	8.77 (0.81)	0.54 (0.81)
Kollumerwaard (PM_{10})	12.85 (0.92)	0.74 (0.92)
Vredepeel (PM_{10})	8.36 (0.89)	0.53 (0.89)

5
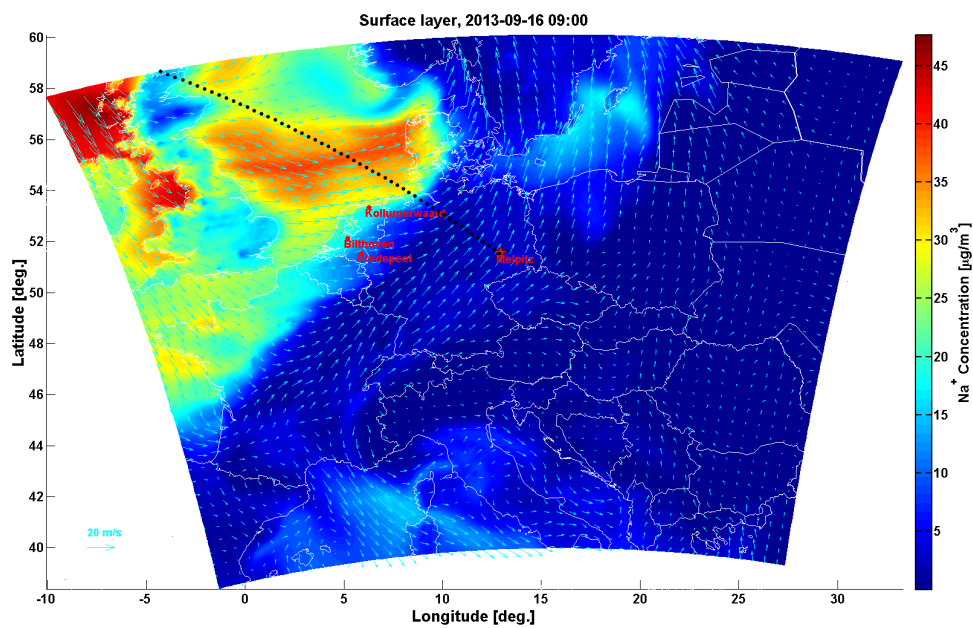
Figure 1. The horizontal distribution of surface Na$^+$ mass concentration in domain 02 at 2013-09-16, 09:00 LT. The light blue arrows indicate the wind field. The locations of 4 EMEP stations (Melpitz, Bilthoven, Kollumerwaard and Vredepeel) are marked. The vertical cross section of dash black line is shown in Figure 5.

Atmospheric
Chemistry
and Physics
Discussions
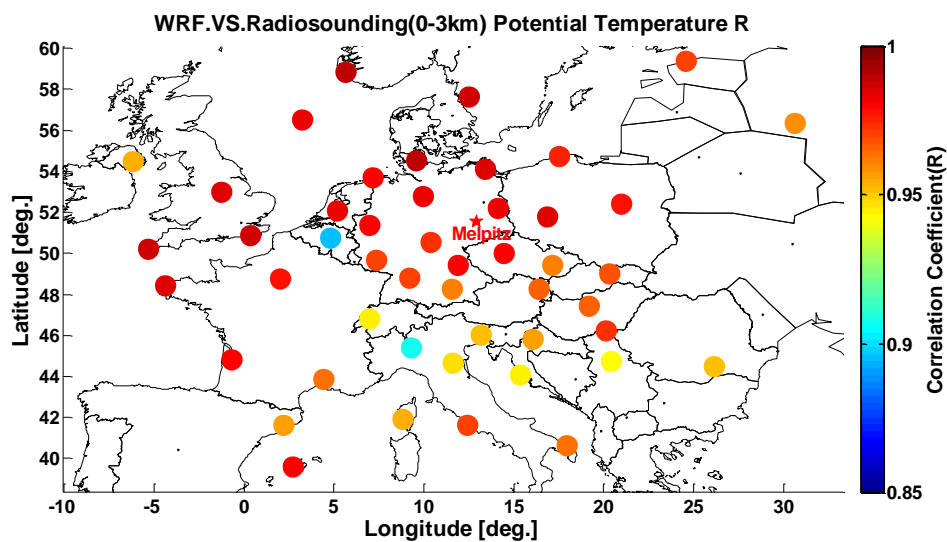
Figure 2. Correlation coefficient (R) map of the potential temperature under 3 km between WRF-Chem model and radio-sounding measurements. Melpitz is marked as red star.
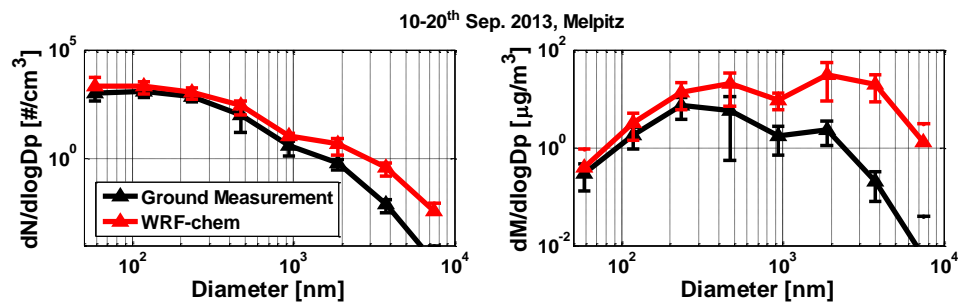
Figure 3. Comparison of Particle Number Size Distribution (PNSD, left) and Particle Mass Size Distribution (PMSD, right) between F-CASE simulation and Melpitz measurements. Model results indicated by the red lines and measurements by the black lines. The result is averaged in the period September 10-20, 2013, the error bar indicate the upper and lower limits.
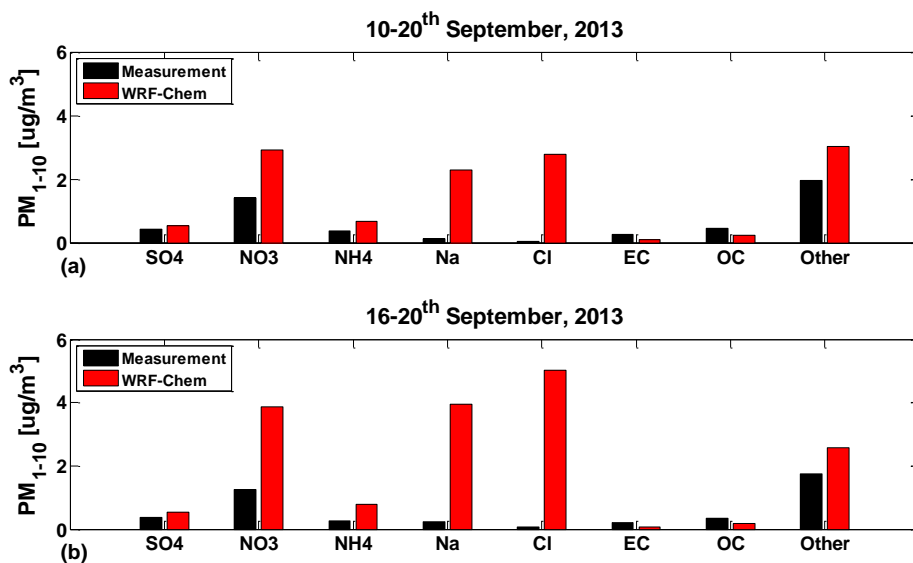
Figure 4. Comparison of coarse mode aerosol (PM_{1-10}) chemistry compounds between WRF-Chem model results and Melpitz measurements. (a) averaged in the HOPE-Campaign period of September 10-20, 2013; (b) averaged in the marine air mass period of September 16-20, 2013.
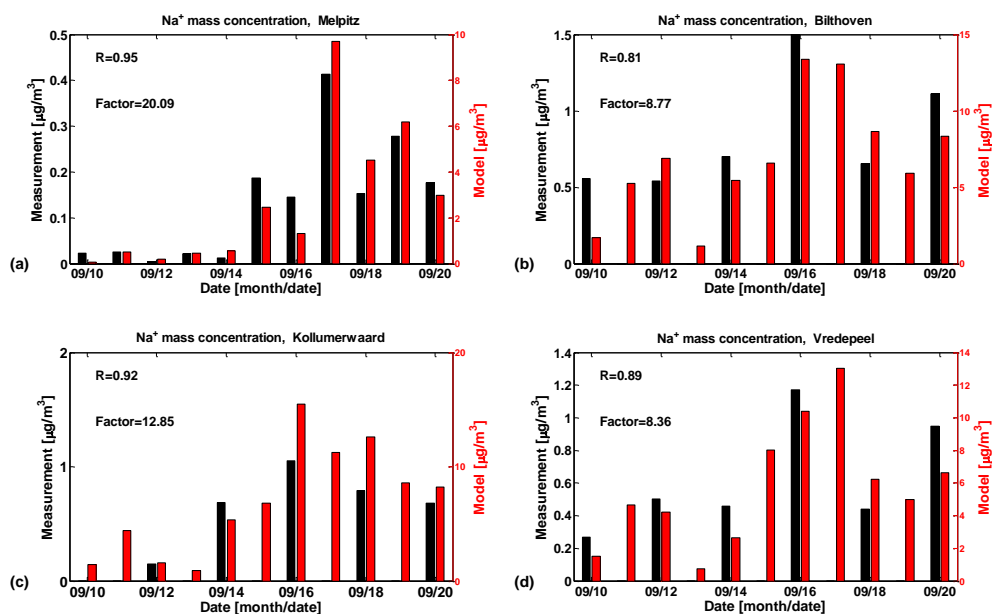
Figure 5. Comparison of Na$^+$ mass concentration between the filter sampler measurement in 4 EMEP stations and WRF-Chem model result. (a) Melpitz; (b) Bilthoven; (c) Kollumerwaard; (d) Vredepeel (locations shown in Figure 1).
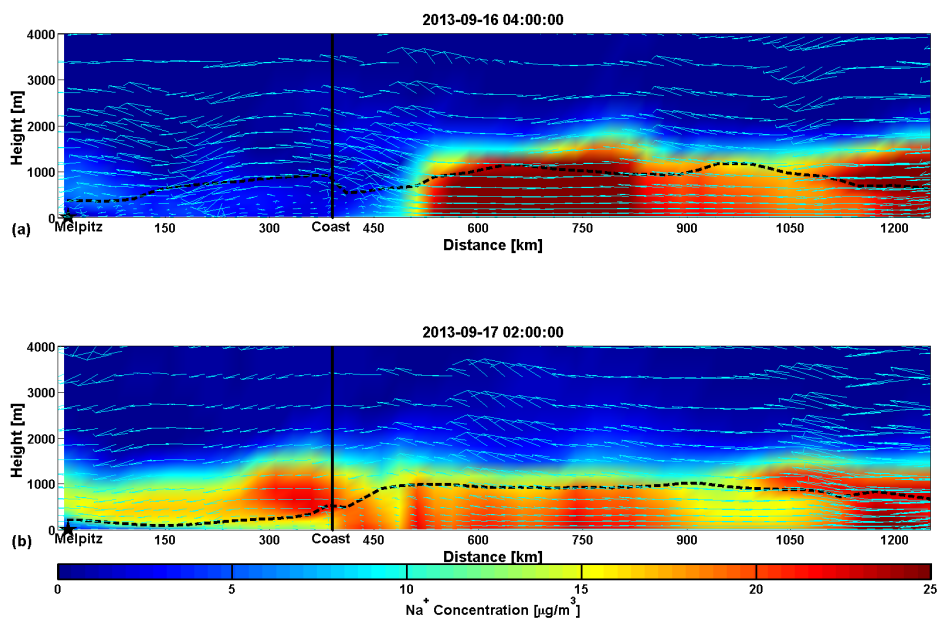
Figure 6. WRF-Chem result of the sea salt (Na$^+$) concentration on the vertical cross section, which is shown by the black dash line in Figure 1. The locations of Melpitz and coast are marked by black five-point star and black solid line. The light blue arrows indicate the wind field, and the black dash line indicates the planetary boundary layer (PBL) height. (a) 2013-09-16, 04:00 LT; (b) 2013-09-17, 02:00 LT.
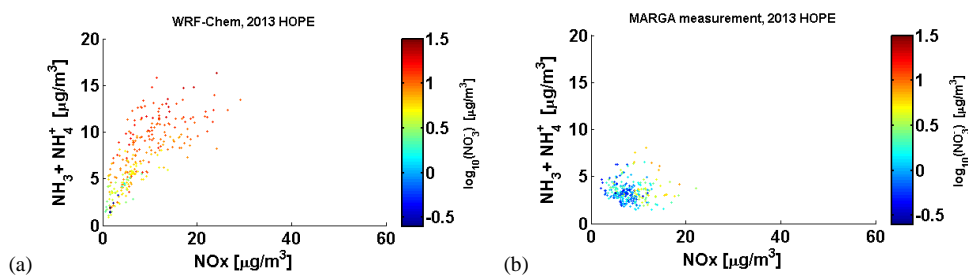
Figure 7. Relationship between nitrate, total ammonia and NOx during September 10-20, 2013 at Melpitz. The color indicates the nitrate mass concentration in logarithmic scale. (a) WRF-Chem model results; (b) MARGA measurement results.
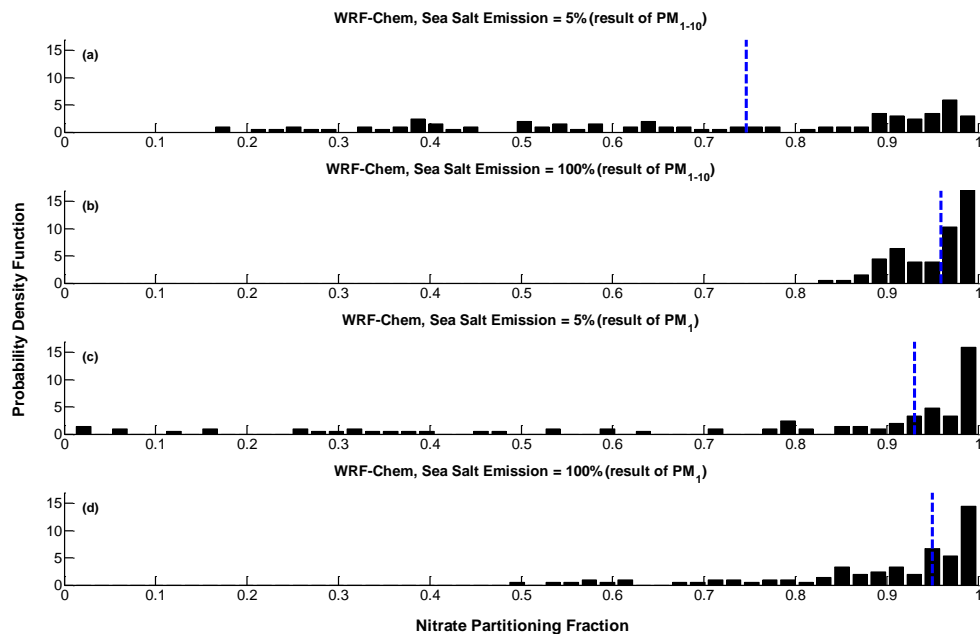
Figure 8. WRF-Chem results of the probability density function of nitrate partitioning fraction (PF_nitrate) at Melpitz in the marine period during September 10-20, 2013. The marine period is defined as the Na^+ mass concentration higher than 1.8 μg/m^3 in F-CASE. The blue dash lines indicate the median value (with 50% probability in both sides). (a) PM_{1-10} result of 5% SSA emission (R-CASE); (b) PM_{1-10} result of F-CASE; (c) PM_1 result of R-CASE; (d) PM_1 result of F-CASE.
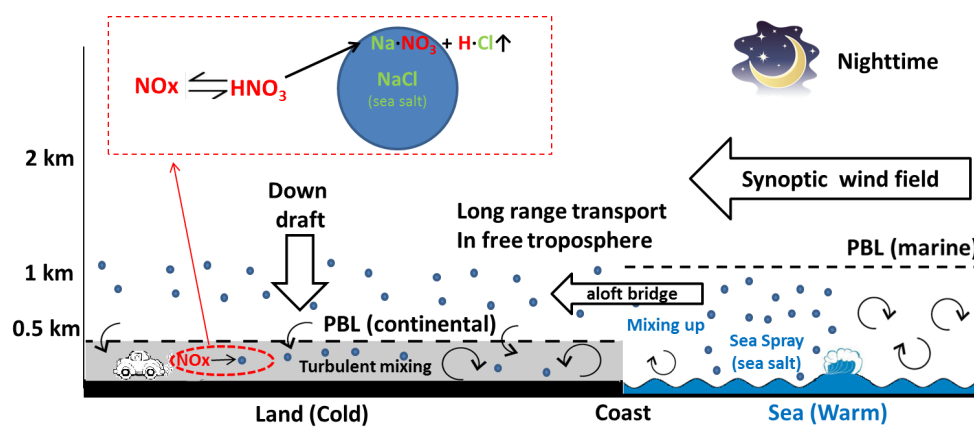
Figure 9. Schematic of sea salt transportation and influence on nitrate formation.